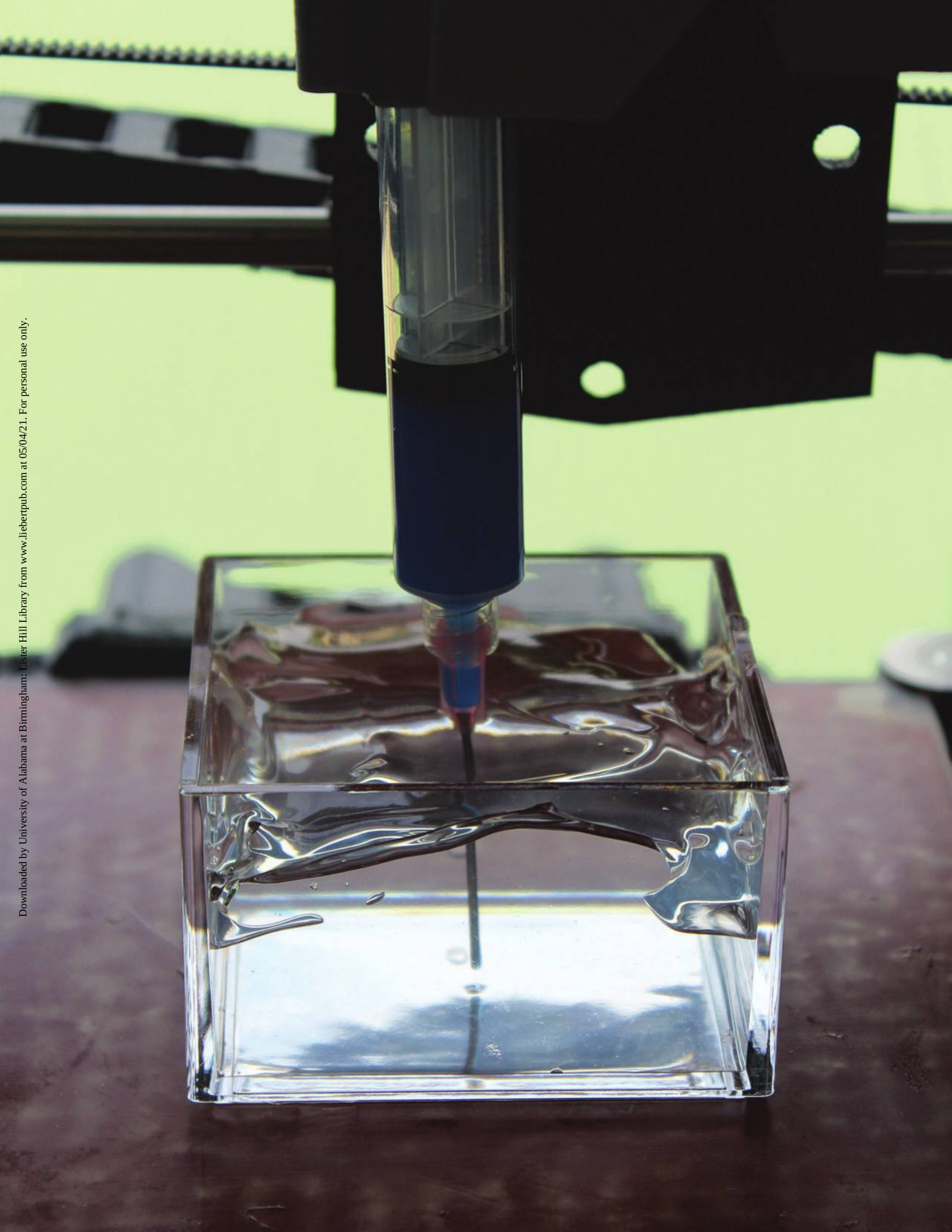

3D PRINTING AND ADDITIVE MANUFACTURING
Volume 6, Number 4, 2019

DOI: 10.1089/3dp.2018.0088

ORIGINAL ARTICLE

Optimization of Silicone 3D Printing with Hierarchical Machine Learning

Aditya Menon,[1] Barnabás Póczos,[2] Adam W. Feinberg,[1,3] and Newell R. Washburn[4]

Abstract

Additive manufacturing of soft materials requires optimization of printable inks, formulations of these feedstocks, and complex printing processes that must balance a large number of disparate but highly correlated variables. Here, hierarchical machine learning (HML) is applied to 3D printing of silicone elastomer via freeform reversible embedding (FRE), which is challenging because it involves depositing a Newtonian prepolymer liquid phase within a Bingham plastic support bath. The advantage of the HML algorithm is that it can predict the behavior of complex physical systems using sparse data sets through integration of physical modeling in a framework of statistical learning. Here, it is shown that this algorithm can be used to simultaneously optimize material, formulation, and processing variables. The FRE method for 3D printing silicone parts was optimized based on a training set with 38 trial runs. Compared with the previous results from iterative optimization approaches using design-of-experiment and steepest-ascent methods, HML increased printing speed by up to 2.5× while retaining print fidelity and also identified a unique silicone formulation and printing parameters that had not been found previously through trial-and-error approaches. These results indicate that HML is an effective tool with the potential for broad application for planning and optimizing in additive manufacturing of soft materials via the FRE method.

Keywords: additive manufacturing, machine learning, design tool, optimization, polymer, 3D printing

Introduction

MAXIMIZING PRINT FIDELITY and speed in additive manufacturing is critical for production optimization, but is challenging because it requires simultaneous modeling of material feedstocks, formulations, and processes.[1] These include fabrication of titanium parts from powder formulations processed by shaped metal deposition,[2] fused deposition modeling of polylactic acid,[3] 3D bioprinting of artificial organs,[4–14] and other novel materials.[15] The large number of variables involved, such as metal powder particle size, melt pool shape and size or filament feeding rate, extrusion width, linear plotting speed and layer thickness or suspension viscosity, crosslinking type and rate, makes traditional optimization approaches based on sequential, iterative experimentation challenging, and thus, there is a critical need for integrated methodologies.

Significant progress has been made in measuring and modeling the effects of material, formulation, or process variables on part attributes. However, there is a need for rapid optimization of these parameters to reduce the number of experiments necessary to fully model the response surface relating manufacturing fidelity and speed with the independent variables. For example, laser melting of metal powders[16] is necessary for microstructure evolution[17] but can lead to thermal deformation[18] that reduces part fidelity. While process maps[19] provide fits over multiple process variables and have been found to provide useful guidance, they rely on intuition of how these process variables are coupled, combined with empirical data fitting to map the manufacturing parameter space.

While the complexity of additive manufacturing suggests that machine-learning tools should be useful, these have two principal shortcomings. The first is that algorithms generally treat systems as black boxes and then attempt to define a response surface based on *de novo* statistical analysis. This then requires extensive data sets to train these models, which can be difficult to generate, especially given the number of variables and time required to probe experimental processing parameters. While it is possible to embed domain knowledge

[1]Department of Materials Science and Engineering, Carnegie Mellon University, Pittsburgh, Pennsylvania.
[2]Department of Machine Learning, Carnegie Mellon University, Gates-Hillman Center, Pittsburgh, Pennsylvania.
Departments of [3]Biomedical Engineering, and [4]Chemistry, Carnegie Mellon University, Pittsburgh, Pennsylvania.

Opposite page: 3D printing of PDMS in a carbopol support bath via FRE process. *Photo Credit:* Aditya Menon.

of physical systems into neural network models, in practice these are designed to work with minimal prior knowledge and are difficult to train.[20]

Hierarchical machine learning (HML) was developed to leverage domain knowledge of complex physical systems when limited data are available.[21] It has a traditional multilayer structure but embeds mathematical functions describing constituent interactions in the system responses to bridge system variables and responses. However, in contrast with process maps, HML uses statistical learning to uncover interactions between independent variables. While this involves regularized regression, advances in these methods have resulted in models that are easier to train and provide mechanistic insight as well as optimization.

Here, HML was applied to the optimization of freeform reversible embedding (FRE) 3D printing of silicone elastomers. FRE is a recently developed method for 3D printing of liquid polymer precursors[22] that involves controlled deposition of a fluid precursor into a supporting aqueous bath characterized by a high viscosity and yield stress, which can be readily extended to bioprinting. Global optimization of this system requires balancing material characteristics and printing parameters, making it representative of the types of additive manufacturing systems for which new design tools are required. Previously, a design-of-experiment methodology was used to optimize the FRE parameters in 3D printing of silicone.[23] In this work, the HML algorithm is established for FRE 3D printing, and a library of fabrication runs is used to train the model. Model refinement and comparisons with purely statistical analysis are discussed.

Materials and Methods

All 3D printing was performed on a Makerbot Replicator™ (MakerBot Industries, LLC, Brooklyn, NY) printer custom modified with a syringe pump extruder, as previously described.[14] Briefly, the thermoplastic extruder was replaced with a custom extruder that holds a removable 10 mL syringe used for silicone deposition. The CAD models for 3D printing were saved in the stereolithography CAD file format and processed into G-code using Replicator G and the Skeinforge slicing engine. Printing speed was varied for different runs in the algorithm. The FRE support bath was placed in a 10 oz cup at the center of the print platform, which was raised to immerse the syringe extruder tip at the bottom. After completion of the print, the cup was placed overnight in a 65°C oven to cure the silicone. Prints were removed with a spatula and washed with running water to remove excess support bath material.

Silicone elastomers (Sylgard 184 and Sylgard 186, Dow Corning) were prepared by mixing the two components at a 10:1 base to curing agent ratio. Silicone elastomers (Dow Corning 3-4241 and Sylgard 567) were prepared by mixing the two components at a 1:1 base to curing agent ratio. A Thinky conditioning planetary centrifugal mixer (Phoenix Equipment, Inc., Rochester, NY) was used for the blending at 2000 RPM for 2 min, followed by an additional 2 min of defoaming at the same speed. The inks were poured into a 10 mL plastic syringe, mounted to the printer.

To train the algorithm, the following variations were explored. (1) Standard needle diameters used were 0.381, 0.406, 1.219, 1.346, 1.75 mm ID, in addition to tapered needle tips with 0.28, 0.63, 0.84, 1.2, and 1.52 mm ID. (2) Inks from Dow Corning used were Sylgard 184, Sylgard 186, Sylgard 567, and Dow Corning 3-4241 at prescribed base to curing agent ratio by weight, respectively.

The support bath was prepared by mixing the bath polymer (Lubrizol) in deionized water with an electric hand blender for 15 min. Specifically, Carbopol® 940 was made at 0.1% w/v, 0.2% w/v, 0.5% w/v, 1% w/v, and 2% w/v. ETD 2020 was made at 0.2% w/v and 1% w/v, and all other polymers (Carbopol 974, Ultrez 10, Carbopol 934, Carbopol 1342, Carbopol 941, Pemulen™ 1621) were prepared at 1% w/v. Before neutralization, dispersions had pH $\sim$3 that was increased to pH 7 using NaOH to form a gel. Before printing, $\sim$80 g of the bath was mixed and defoamed in the Thinky conditioning mixer using the same setting as the inks.

The CAD model of the hollow cylindrical tube design, which was 3D printed inside the support bath, was obtained from the Thingiverse repository.

Rheological analysis was conducted using a Bohlin Instruments Gemini 200 rheometer (Malvern Instruments Ltd., United Kingdom) with a cone and plate geometry (4° cone angle, 40 mm diameter) and 150 μm gap size. The shear stress and viscosity were measured as a function of shear rate in the 0.005–500 Pa range. The amplitude sweep test was done at a frequency of 1 Hz for strains of 0.001–10%. To determine the storage (G′) and loss (G″) modulus, the frequency sweep test was conducted from 0.001 to 50 Hz at 0.01% strain. All experiments were performed under isothermal conditions (25°C). The rheological parameters of the ink and bath materials are tabulated in the Data in Brief file.

The FRE process

FRE is a 3D printing technique developed for soft materials where liquid precursors are extruded into a support bath that prevents gravity-driven flow during the layer-by-layer process (Fig. 1a).[14,22,24] The support bath is composed of a carbomer hydrogel that behaves as a Bingham plastic, yielding as a viscoelastic liquid to the extruder but recovers rapidly to support the green form during printing. After printing, the silicone elastomer was cured at 65°C, and then, the printed part was manually removed from the support bath and washed with water to remove residual bath polymer.

The interaction of the needle of the extruder with the support bath is complex, especially at high shear rates associated with rapid printing.[25] Motion of the needle generates an air gap at the bath surface and localized fluidization of the hydrogel occurs near the tip, both of which can influence feature resolution and interlayer connectivity. The silicone ink is a Newtonian fluid with a viscosity much lower than that of the bath, even in the postyield state, and viscosity mismatch can result in fingering instabilities[11] that can impact printing fidelity. The recovery time of the bath depends on the yield stress, viscosity, and recovery time following cessation of shear, all of which depend sensitively on both polymer chemistry and polymer concentration. It should be noted that in this work, these complex shear-dependent effects of the needle and ink on the bath properties are captured in a single descriptor based on the bath viscosity at the yield point. Furthermore, the process variables of needle diameter, volumetric flow rate of the silicone ink, needle velocity, and retraction distance, preventing ink over extrusion into the bath, can all have complex effects on printing. Global optimization of the FRE printing method requires simultaneous tuning of all these variables to optimize print fidelity and speed,

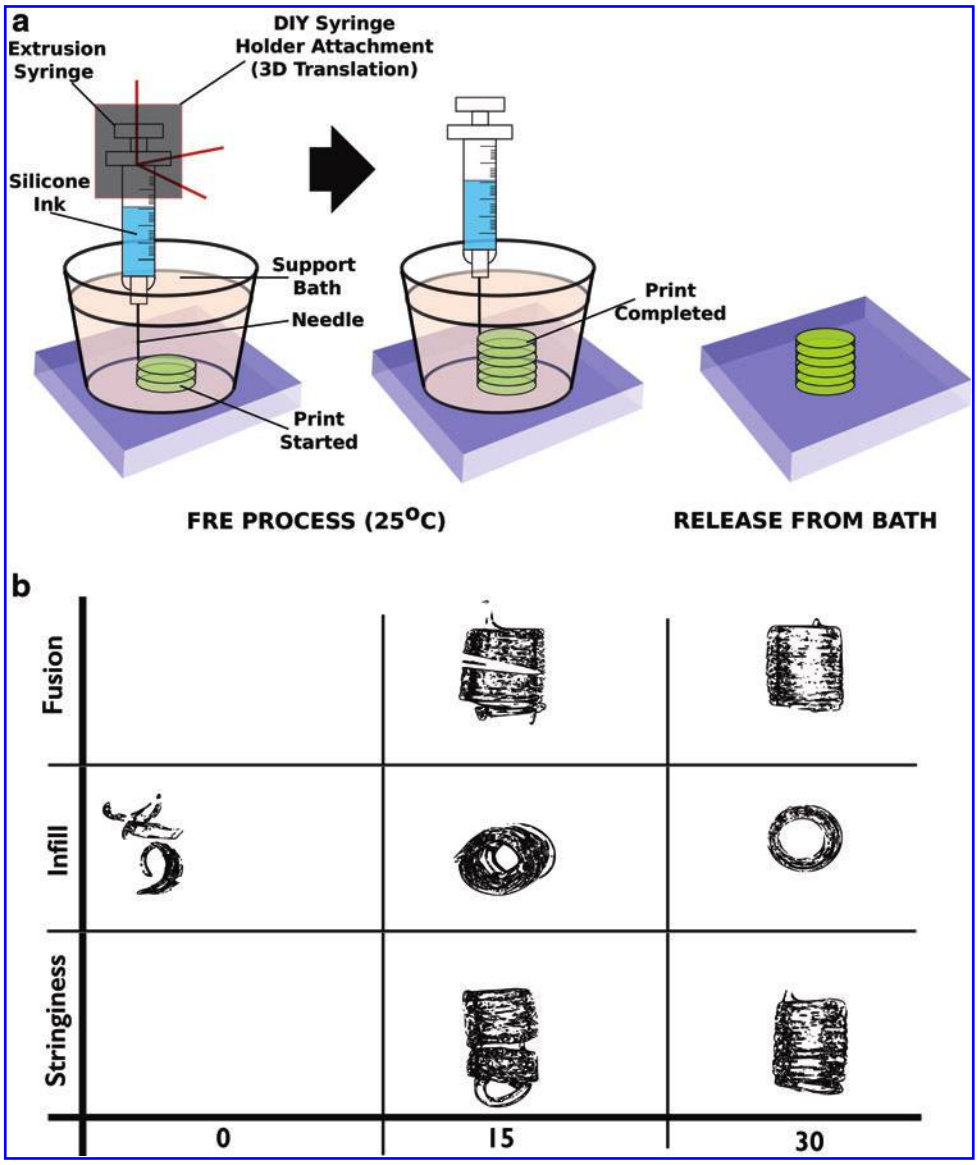

FIG. 1. **(a)** 3D printing polydimethylsiloxane elastomer in a hydrophilic support bath via FRE.[11] **(b)** Representative examples of various run samples rated from lowest scores (*left*) to highest scores (*right*) in three categories.[14] FRE, freeform reversible embedding. Color images are available online.

but in this first application of HML, a subset of the complete set of variables was explored in simplified representations for the purposes of building a basic modeling and demonstrating its potential in complex manufacturing processes.

System responses

The data set used to train the algorithm contained 38 prints of a hollow cylindrical tube (D = 10.8mm, H = 13.5mm), and the training set is summarized in Supplementary Table S1. Based on a standard rubric,[23] each print was scored out of 10 possible points in 3 categories: ''layer fusion,'' which is characteristic of the adhesion between print layers, ''stringiness,'' which is the adhesion, specifically for the first few layers that hang loosely in case of a bad score, and ''infill,'' which is the bulging or collapse of material around the middle layers of the cylindrical form. The system response, denoted by print score P, to be optimized with the HML model is a sum of these three components of the rubric with a maximum score of 30.

Experimental variables

Experimental variables are chosen for the system to achieve a certain response and are broadly grouped into three categories of bath (bath material and bath concentration), ink (ink material), and printer (flow rate, needle size, and retraction distance) variables. The flow rate is the ink velocity while extruding out of the syringe, the needle diameter relates to the individual layer height in the printed part, and the retraction distance is the distance that the ink is pulled back in the syringe pump with a reverse motion of the stepper motor after each print to avoid ink leakage before starting the next print.

Regularized regression with Lasso

A critical issue in statistical learning is identifying an optimal variable set that models data in the training set and also predicts responses in test data.[26] An excessively large variable set results in overfitting the training set, which provides an accurate prediction for responses from these data but

performs poorly in modeling test data. In contrast, using too few variables to describe system responses results in poor fits of the training set—referred to as underfitting—but better predictions of new data in a test set. A powerful tool for determining optimal variable sets in regression analysis is the least absolute shrinkage and selection operator (Lasso).[22]

$$\min_w(||Xw - y||_2^2 + \lambda||w||_1) \quad (1)$$

This cost function is minimized by simultaneously minimizing the difference between the predicted (Xw) and actual values (y), as well as the set of coefficients. The latter includes a tuning parameter λ that systematically drives coefficients to zero, thereby reducing the size of the set of regression coefficients. The term $||w||$ in equation 1 represents the sum of regression coefficients, which will be minimized to give a minimal variable set that can still accurately model the training data. In this work, Lasso was used to explore the functional relationship between the underlying physical variables and the system responses, effectively a pure statistical learning model, as well as in the HML algorithm.

The HML algorithm

The algorithm developed for optimization of the FRE printing method is shown in Figure 2. The top layer represents complex system responses to be optimized, which in FRE are the three components (layer fusion, stringiness, and infill) of the scoring rubric that represent print fidelity. As noted, print speed is maximized by setting the ink flow rate and needle speed to an allowed range of values and identifying parameter settings within this range that maximize print speed while maintaining print fidelity. The system response to be optimized is called print score, P (scored out of 30), which is a sum of individual scores of layer fusion, stringiness, and infill, each scored out of 10, consistent with previous work in this area.[23]

The central layer of the algorithm represents the physical forces and interactions that underlie print fidelity. These include the bath viscosity as a function of polymer concentration and specific viscosity, ink viscosity, and the flow rate as a function of pressure drop. Initial versions of the algorithm did not include an interfacial tension, which can result in Rayleigh instabilities and breakup of the silicone ink, but these were included in subsequent versions.

The bottom layer of the algorithm represents independent (experimental) variables, some of which were discrete, such as the type of ink or bath material that was used, and some were continuous, such as bath concentration or ink flow rate. The algorithm handles each variable separately and ultimately parametrizes system responses as a function of all of them.

The algorithm was described in detail previously.[21] Briefly, the complex system responses in the top layer were probed as a function of the experimental variables in the bottom layer. This generates the training set used in teaching the model. The constituent forces and interactions were then measured as a function of the experimental variables to provide parametrized expressions that relate experimental variables (bottom layer) to constituent forces (middle layer). Separately, the system responses (top layer) are statistically decomposed in terms of the values of the constituent forces using regularized regression. In hierarchical integration, the system responses are finally expressed in terms of the experimental variables through reparametrization of the expression for system response, originally represented in terms of forces, by the experimental variables. Then, global maxima or minima can be identified subject to application-specific constraints to identify values of experimental variables that optimize system responses.

In this research, all computational work was performed with the MATLAB and R software suites. The R package was used for statistical modeling and MATLAB was used for optimization and generating plots.

Results and Discussion

Statistical evaluation of training data

Before applying the HML algorithm, the data relating print fidelity to the experimental variables were explored using Lasso to evaluate whether the training set of 38 prints was sufficient to develop a model to predict print fidelity. In a previous study on

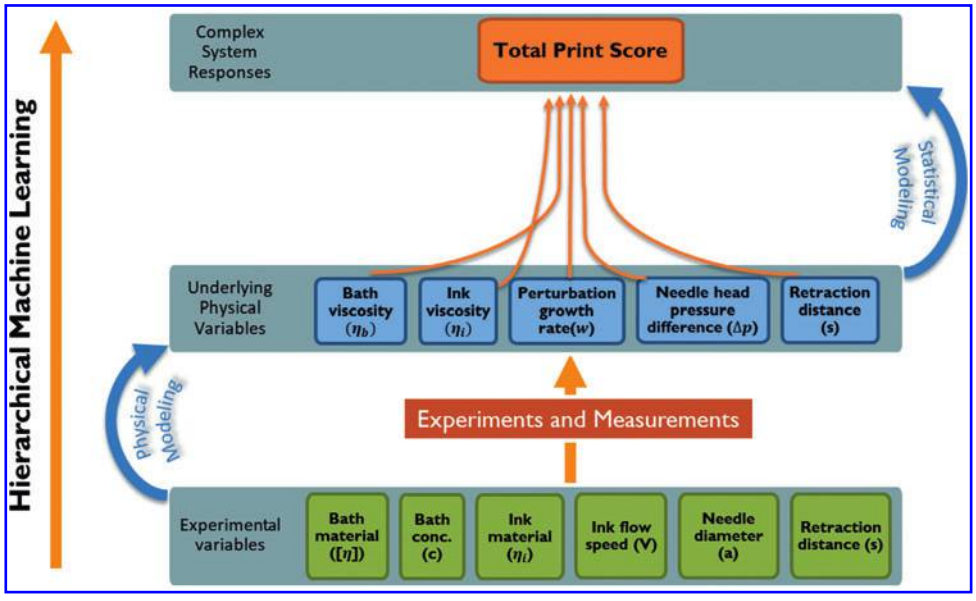

FIG. 2. Schematic representation of HML model of the FRE process. HML, hierarchical machine learning. Color images are available online.

Table 1. Comparison of Optimized Values from Pure Statistical Prediction and Previously Obtained Optimum Values Through Expert-Guided Steepest-Ascent Methods

	Bath concentration (w/v%)	*Ink viscosity (Pa.s)*	*Layer height (mm)*	*Flow rate (mm/s)*	*Retraction distance (mm)*	*Bath material*	*Ink material*
Steepest-descent optimization[23]	0.01	3.50	0.9652	10	0.3	Carbopol® 940	Sylgard 184
Lasso prediction	0.01	3.50	0.974	10.47	0.53	Carbopol 940	Sylgard 184

this system,[23] expert-guided steepest-ascent methods were developed to optimize the experimental variables by sequential, iterative analysis.[23] Here, the same data, based on combinations of experimental variables and the corresponding printing score, were analyzed using Lasso, allowing for ranges of variables based on experimental constraints. Of particular importance was print speed, which was allowed to vary from 0 to 50 mm/s.

The results from Lasso regression on our training data set are tabulated in Table 1. It is seen that there is generally close agreement on the predictions of steepest-descent optimization and regularized regression, which suggests that the response surface established from this small training set was explored as accurately as possible using both methods. However, there may be hidden synergies between variables that were not captured by purely graphical or statistical methods, and HML was then applied to explore whether new insights could be gained from integration of physical modeling into a statistical learning framework.

Sensitivity analysis of experimental variables

A critical component of the HML methodology is determining the range over which the experimental variables can be set and still achieve optimal responses. In complex systems, competing interactions make it impossible to reach performance metrics based on maximization of a small number of variables. Rather, optimal solutions involve balancing variables within ranges, and in these systems, it is the synergies between variables that are exploited to achieve optimization.

Sensitivity analysis was performed to establish ranges over which experimental variables could be set. These results were also the basis for determining the set of underlying physical processes and interactions that were embedded in the middle layer of the HML algorithm. In exploring the dependence of print fidelity on needle diameter, it was observed that needles with narrower inner diameter resulted in fluid instabilities that led to breakup of the polydimethylsiloxane ink into droplets. Representative print is shown in Figure 3a where it is observed that a noncontiguous form was produced. This led to the incorporation of a Rayleigh instability mechanism as part of the HML model for the FRE process and limited the range of needle ID used in printing. In Figure 3b it can be seen that perturbation growth rate decays rapidly with increasing needle diameter. However, based on different concentrations of Carbopol 940

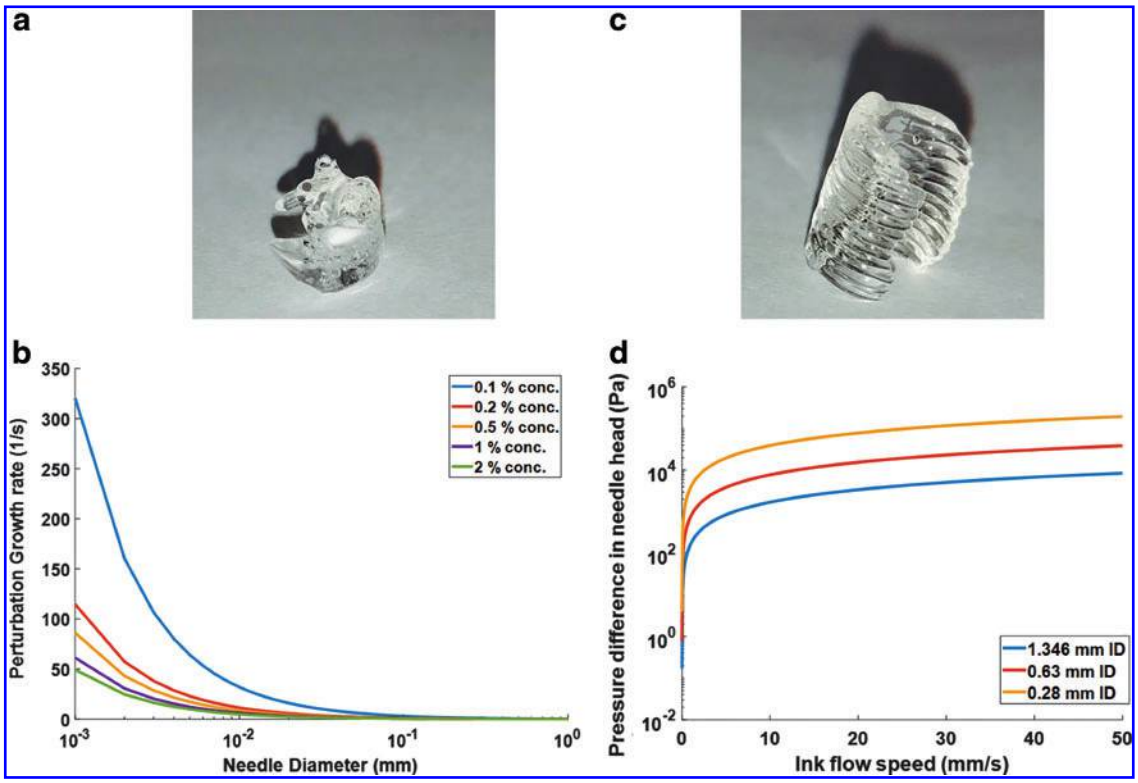

FIG. 3. **(a)** Too small needle diameter results in fluid breakup and uneven print. **(b)** Figure showing perturbation growth rate versus needle diameter (log scale) at various concentrations of Carbopol® 940 support bath. **(c)** Too fast flow rate creates a lack of volume on one side of the print. **(d)** Figure showing pressure difference in needle head (log scale) versus ink flow speed at various needle IDs. Color images are available online.

Table 2. Representative Functions for Physical Models Used in the Hierarchical Machine Learning Model

Huggin's equation[4]	$\eta_b = 1 + [\eta]c + k_H [\eta]^2 c^2$
Fluid thread breakup in higher external viscous medium[5]	$w = \frac{\sigma(1-k^2a^2)}{(2a\eta_b)\left(k^2a^2+1-k^2a^2K_0^2(ka)/K_1^2(ka)\right)}$
Hagen–Poiseuille law	$V = \frac{\Delta p R^2}{8\eta_i l}$

support bath, it can start at a high growth rate (c). Too fast flow rate creates a lack of volume on one side of the print. In Figure 3c flow rate was increased to five times of the optimum speed and subsequent print started to lack volume along one side of the printed tube. The lack of material flow at a particular position occurs in every layer of the print, which could be attributed to the pressure difference developed at the needle head due to increased flow rate. Figure 3d shows that the pressure evolves rapidly at needle head with increasing flow rate at different needle diameters, especially in thinner needle diameters.

Parametrization of underlying physical variables by experimental variables

Connecting the bottom layer of the HML model with the middle layer requires parametrization of the underlying physical forces and interactions by the experimental variables. This was accomplished using physical models that capture the underlying forces and then experimentally determining necessary coefficients in the models. In modeling the FRE process, the ink viscosity (η_i) and retraction distance (s) were taken as pure numerical variables, but the rheological properties of the bath (η_b), perturbation growth rate due to Rayleigh instability in the ink fluid thread coming out of the nozzle (w), and pressure dependence of the ink flow rate (Δp) were parametrized by experimental variables. The functions for these are shown in Table 2.

The viscosity of the bath was variable and was modeled based on a simplified form of Huggins equation,[27] ignoring the quadratic and higher order terms where viscosity only depends on the concentration and intrinsic viscosity of the polymeric bath material.

To model fluid thread breakup, a Rayleigh–Plateau instability was incorporated in which perturbations develop on the free surface of the fluid, growing rapidly over time and resulting in unstable fluid flow for viscous fluids. Extruding a low-viscosity material into a high-viscosity medium can be represented by the work done by Tomotika,[28] who described in detail how the perturbation growth rate becomes only a function of the initial radius of the fluid thread, the perturbation wavelength, the surface tension of the thread, and the viscosity of the external environment, which can be accurately modeled using second-order Bessel functions of the second kind. In our model, it was assumed that the perturbation wavenumber remains constant for all conditions, which was represented as a unit quantity here. The interfacial tension values for different silicone inks generally range between 20 and 30 mN/m,[29,30] and the average was used. However, the most important variable parameters for us would be length scale (fluid thread radius) and viscosity of support bath. The final independent variable was the pressure used to drive flow of the ink. Based on Hagen–Poiseuille law, the flow rate was assumed to be directly proportional to the pressure difference and needle size and inversely to ink viscosity and length of the needle.

Statistical modeling of the system responses by underlying physical variables

In HML, the system responses are expressed in terms of the underlying physical variables in the middle layer, and their contribution and couplings are determined through statistical learning. Here, regularized regression was used to identify the underlying physical variables and their combinations that most strongly determine system responses. The simplest representation of variable coupling was to use the products of the underlying variables in the middle layer, and this was utilized here.

Based on five underlying physical forces or interactions and ten cross-terms between them, Lasso with ''leave one out'' cross-validation (LOOCV) was used to identify an optimal

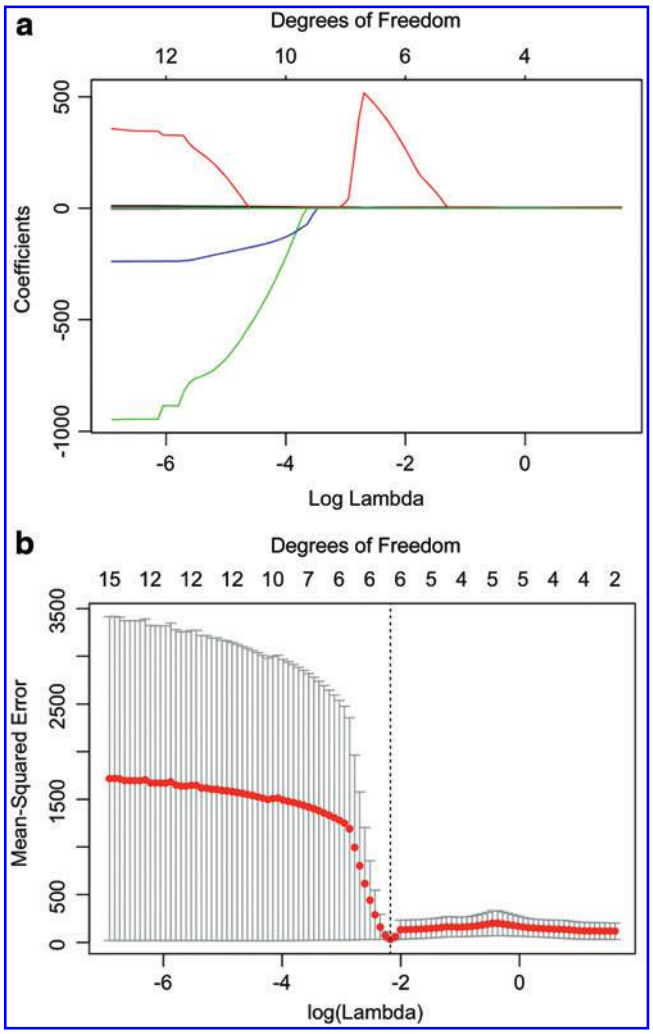

FIG. 4. **(a)** Lasso path for determining the minimal variables with best fit to represent the total score of a print as a complex function in bath viscosity, ink viscosity, perturbation growth rate, pressure difference, and retraction distance. Starting with the full basis set of 15 variables, Lasso increasingly suppressed regression coefficients as lambda was increased. The *colored lines* represent the magnitudes of various coefficients with respect to the varying values of lambda. **(b)** Cross-validation result plotting the validation mean squared prediction error against lambda values. The *dotted lines* represent the value of lambda providing the balance between best fit versus predictive power. Color images are available online.

variable set that balanced modeling of the data in the training set with predicting the responses to new data in a test set. The results are shown in Figure 4 in which the Lasso trajectories are plotted as a function of the discriminating parameter λ to identify combinations of middle-layer variables that best represent system responses shown in Figure 4a. Here, it can be seen that the magnitude of coefficients, as well as the selection of coefficients, is changing based on decreasing values from right to left. To select the appropriate value of λ and find the perfect balance between underfitting and overfitting, cross-validation was performed. In Figure 4b shows the results of LOOCV in which the mean-squared error is plotted as a function of λ, which provides guidance on balancing overfitting (small λ) and underfitting (large λ). In leave-one-out cross-validation, at one value of λ, the model was created from all data points except one and tested against it for prediction accuracy. This step was repeated for all data points and a mean squared error (MSE) was calculated for each value of λ. Thus, the value of lambda, which provided the lowest MSE, was used for determining the coefficients and the respective magnitudes.

The final variables are shown in equation 2. It should be noted that the R software standardizes all variables by the ratio of difference from mean to the standard deviation before performing regularized regression and then rescales the coefficients to their nonstandardized values. This makes the relative magnitude of each coefficient unimportant; only the product of the coefficient and its variable determines the relative contribution to the system responses.

$$\begin{aligned} \mathrm{P} = {} & 0.122\eta_b + 5.349\eta_i + 2.227s - 0.028\eta_b\eta_i \\ & - 0.004w\Delta p + 344.3ws \end{aligned} \tag{2}$$

Variables and combinations of variables without a regression coefficient were found to have less predictive power than those that Lasso and LOOCV analyses retained. The magnitude of each coefficient that was included in the regression fit represented its relative contribution, and the sign indicated whether it was positively or negatively correlated with the scoring rubric that quantified print fidelity. For example, the bath and ink viscosities were positively correlated with print fidelity, but the coupling between them was negatively correlated. This can be interpreted as predicting that increasing either ink or bath viscosity will improve print fidelity, possibly through reducing flow of the form before crosslinking, but increasing both without bound would decrease printability and print fidelity.

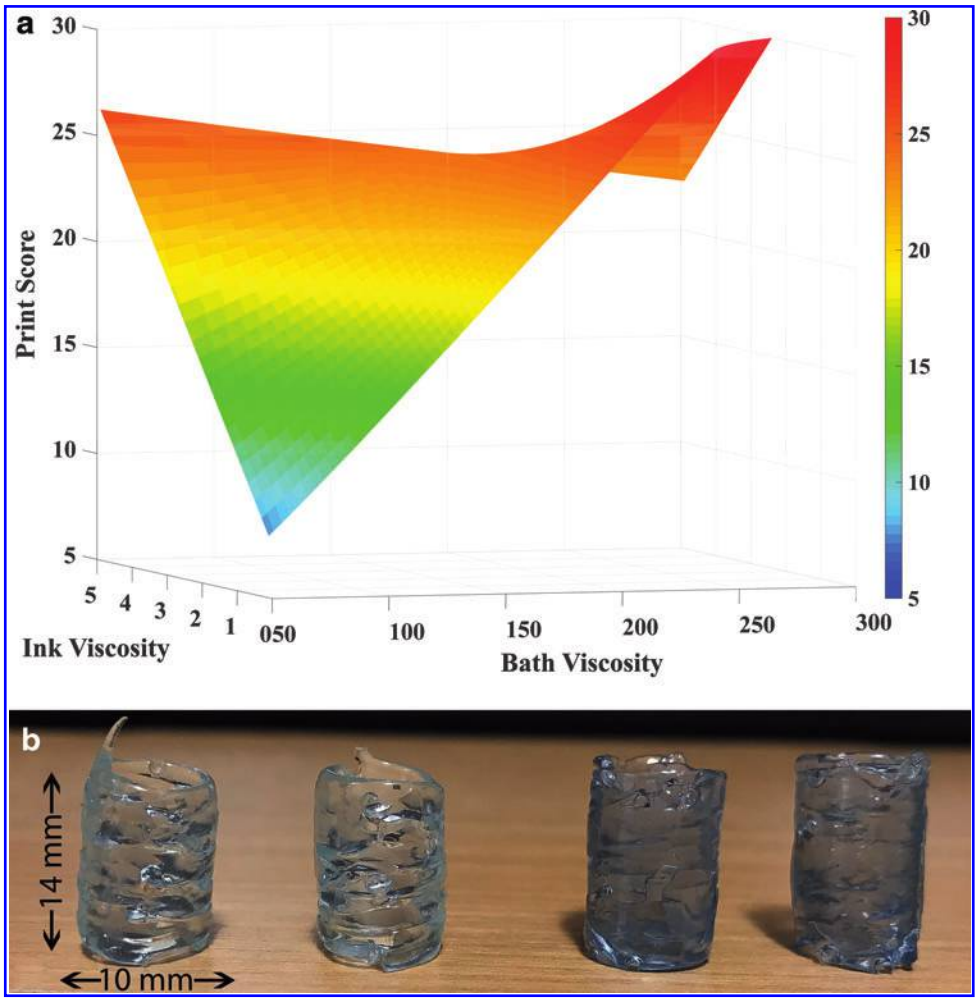

FIG. 5. **(a)** A response surface generated from the final polynomial equation for print score with respect to ink viscosity and bath viscosity while keeping needle size, flow rate, and retraction distant constant at 0.9652 mm, 10 mm/s, and 0.3 mm, respectively, which were optimal for the highest print speed. **(b)** Here, from *left* to *right*, first two prints are previous best runs for Dow-Corning 3-4241 ink and the next two runs are from HML prediction two for the same ink. Color images are available online.

Table 3. Sets of System Variables Optimized by Expert-Guided Steepest-Ascent Methods and Predicted System Variables Post Constrained Nonlinear Minimization of Hierarchical Machine Learning Model in MATLAB

	Print score	*Bath concentration (w/v%)*	*Ink viscosity (Pa.s)*	*Layer height (mm)*	*Flow rate (mm/s)*	*Retraction distance (mm)*	*Bath material*	*Ink material*
Previous best run	29	0.01	3.50	0.9652	10	0.3	Carbopol 940	Sylgard 184
Previous best run	26	0.01	0.42	0.9652	10	0.3	Carbopol 940	Dow Corning 3-4241
HML prediction 1	28	0.012	3.50	0.93	22.71	0.64	Carbopol 940	Sylgard 184
HML prediction 2	28	0.008	0.42	1.27	25.98	0.49	Carbopol 940	Dow Corning 3-4241

HML, hierarchical machine learning.

It is also interesting to note the classes of variables that were retained by the Lasso trajectory. Only three single variables were included: bath viscosity (η_b), ink viscosity (η_i), and retraction distance (s). However, the Rayleigh instability of the ink stream in the bath, measured through perturbation growth rate (w) and the pressure-drop across the needle (Δp), formed a composite variable based on the product, and the fluid instability also coupled with the retraction distance. Thus, all independent variables were represented. However, the only term that coupled material variables and process variables was the product of fluid instability length and the retraction distance. This suggests that material and formulation variables form a related class, while processing variables are a separate class. One potential implication of this is that the printing variables can be separately optimized from the material and formulation variables, which would allow for separate optimization of material feedstocks when applying the FRE process to new systems. While the model presented here is not universal (nor even complete in terms of including all possible variables that define FRE print fidelity), the general structure of the model could be used to efficiently train the algorithm in optimization of 3D printing by FRE.

Constrained nonlinear minimization of the HML polynomial

Optimization of the FRE process for silicone 3D printing can be accomplished through reparametrization of the function representing print fidelity in terms of the underlying physical forces (Eq. 2) by the representation of these forces in terms of the independent variables. Then identification of global extrema identifies variable settings that maximize this function, subject to application constraints.

The experimental variables were represented as a six-dimensional vector (or six-tuple) and the parametrized space for print fidelity P was therefore also six-dimensional. While print speed was determined by the independent variable Δp, optimization can be constrained to identify perfect scores ($p = 30$) for print fidelity with the greatest value for Δp. Using the same bath and ink materials that were identified through previous optimization runs,[23] HML identified values of bath concentration, layer height, and retraction distance that were predicted to result in maximum print scores with a print speed that was more than $2\times$ greater than previous settings.

Printing low-viscosity inks is a challenge in FRE, and the HML algorithm was then used to identify conditions for which high print fidelity can be obtained. The algorithm predicted that bath viscosity was an important factor in modulating the effects of low ink viscosity through the cross-term $\eta_b\eta_i$ in equation 2. The response surface for the print score as a function of bath and ink viscosities is shown in Figure 5a. While optimization of FRE requires elucidating the interplay of a large number of variables, the interplay between ink and bath properties is illustrative of the insight that this algorithm can provide along with the quantitative performance. For example, it was observed that low-viscosity silicone inks were challenging to print using FRE, and HML predicts that this is due to the interplay with bath properties where less viscous inks require a bath with higher viscosity to maintain high print fidelity. The results are tabulated in Table 3 and representative prints are shown in Figure 5b.

Comparison of approaches

The results presented here indicate that HML provides a richer representation of the response surface relating print fidelity and speed with experimental variables than expert-guided steepest ascent. This latter approach does not model synergies between variables when the response space is complex, involving hidden couplings between variables, but rather will generally fit these response surfaces with polynomials or other smoothly varying functions. To accomplish this, HML offers two central advantages. As with any machine-learning methodology, variable selection and dimensionality reduction in HML are critical. This leads to identification of variables that are central determinants of system responses, allowing for more predictions of responses outside of the original training set. The second advantage is specific to HML. The forces that are represented in the middle layer of the algorithm can be considered latent variables that actually determine system responses. Parametrization of these latent variables by the experimental variables allows HML to create a virtual model of the system in which the dependences (and interdependences) of variables in the middle and bottom layers express the complex synergies that make traditional modeling approaches so challenging.

Conclusions

Machine learning was used to model 3D printing of silicone elastomer in the FRE process. Through integration of physical models, the HML algorithm predicted processing conditions for increasing print speed by twofold or using low-viscosity inks that previously led to forms with a low print score. This was based on sparse training sets having only 38 elements for a system with 6 independent variables that would require a significantly larger training set for traditional machine-learning algorithms. HML could be a useful tool in FRE where the complex interplay between large parameter spaces of material, formulation, and processing variables makes it difficult to determine the response surface and achieve global optimization.

Acknowledgments

The assistance of Sara Abdollahi in sample preparation and print scoring is gratefully acknowledged. This work was supported, in part, by funding from the National Science Foundation (CBET-1510600) to N.R.W. and the Disruptive Health Technology Institute at Carnegie Mellon University to A.W.F.

Author Disclosure Statement

B.P. and N.R.W. have started a company to explore commercial applications of the algorithm described here, which represents a potential conflict of interest.

Supplementary Material

Supplementary Table S1

References

1. Truby RL, Lewis JA. Printing soft matter in three dimensions. Nature 2016;540:371–378.
2. Baufeld B, Biest O van der, Gault R, *et al.* Manufacturing Ti-6Al-4V Components by shaped metal deposition: microstructure and mechanical properties. IOP Conf Ser Mater Sci Eng 2011;26:012001.
3. Giordano RA, Wu BM, Borland SW, *et al.* Mechanical properties of dense polylactic acid structures fabricated by three dimensional printing. J Biomater Sci Polym Ed 1997;8:63–75.
4. Chia HN, Wu BM. Recent advances in 3D printing of biomaterials. J Biol Eng 2015;9:4.
5. Murphy SV, Atala A. 3D bioprinting of tissues and organs. Nat Biotechnol 2014;32:773–785.
6. Highley CB, Rodell CB, Burdick JA. Direct 3D printing of shear-thinning hydrogels into self-healing hydrogels. Adv Mater 2015;27:5075–5079.
7. Guvendiren M, Molde J, Soares RMD, *et al.* Designing biomaterials for 3D printing. ACS Biomater Sci Eng 2016;2:1679–1693.
8. Bandyopadhyay A, Bose S, Das S. 3D printing of biomaterials. MRS Bull 2015;40:108–114.
9. Zhu W, Ma X, Gou M, *et al.* 3D printing of functional biomaterials for tissue engineering. Curr Opin Biotechnol 2016;40:103–112.
10. Jakus AE, Rutz AL, Shah RN. Advancing the field of 3D biomaterial printing. Biomed Mater 2016;11:014102.
11. Wang S, Lee JM, Yeong WY. Smart hydrogels for 3D bioprinting. Int J Bioprinting 2015;1:3–14.
12. Melchels FPW, Domingos MAN, Klein TJ, *et al.* Additive manufacturing of tissues and organs. Prog Polym Sci 2012;37:1079–1104.
13. Stanton MM, Samitier J, Sánchez S. Bioprinting of 3D hydrogels. Lab Chip 2015;15:3111–3115.
14. Hong S, Sycks D, Chan HF, *et al.* 3D Printing: 3D Printing of highly stretchable and tough hydrogels into complex, cellularized structures. Adv Mater 2015;27:4034.
15. Lee J-Y, An J, Chua CK. Fundamentals and applications of 3D printing for novel materials. Appl Mater Today 2017;7:120–133.
16. Roberts IA, Wang CJ, Esterlein R, *et al.* A three-dimensional finite element analysis of the temperature field during laser melting of metal powders in additive layer manufacturing. Int J Mach Tools Manuf 2009;49:916–923.
17. Jia Q, Gu D. Selective laser melting additive manufacturing of Inconel 718 superalloy parts: densification, microstructure and properties. J Alloys Compd 2014;585:713–721.
18. Paul R, Anand S, Gerner F. Effect of thermal deformation on part errors in metal powder based additive manufacturing processes. J Manuf Sci Eng 2014;136:031009.
19. Beuth J, Fox J, Gockel J, *et al.* Process mapping for qualification across multiple direct metal additive manufacturing processes. Proc 24th Int SFF Symp 2013;1:655–665.
20. Thompson ML, Kramer MA. Modeling chemical processes using prior knowledge and neural networks. AIChE J 1994; 40:1328–1340.
21. Menon A, Gupta C, Perkins KM, *et al.* Elucidating multiphysics interactions in suspensions for the design of polymeric dispersants: A hierarchical machine learning approach. Mol Syst Des Eng 2017;2:263–273.
22. Hinton TJ, Jallerat Q, Palchesko RN, *et al.* Three-dimensional printing of complex biological structures by freeform reversible embedding of suspended hydrogels. Sci Adv 2015;1:e1500758–e1500758.
23. Abdollahi S, Davis A, Miller JH, *et al.* Expert-guided optimization for 3D printing of soft and liquid materials. PLoS One 2018;13:e0194890.
24. Hinton TJ, Hudson A, Pusch K, *et al.* 3D Printing PDMS elastomer in a hydrophilic support bath via freeform reversible embedding. ACS Biomater Sci Eng 2016;2:1781–1786.
25. LeBlanc KJ, Niemi SR, Bennett AI, *et al.* Stability of high speed 3D Printing in liquid-like solids. ACS Biomater Sci Eng 2016;2:1796–1799.
26. Tibshirani R. Regression Selection and Shrinkage via the Lasso. J R Stat Soc B 1996;58:267–288.
27. Pamies R, Hernández Cifre JG, del Carmen López Martínez M, *et al.* Determination of intrinsic viscosities of macromolecules and nanoparticles. Comparison of single-point and dilution procedures. Colloid Polym Sci 2008;286:1223–1231.
28. Tomotika S. On the instability of a cylindrical thread of a viscous liquid surrounded by another viscous fluid. Proc R Soc A Math Phys Eng Sci 1935;150:322–337.
29. Baier RE. Correlations of materials surface properties with biological responses. J Surf Eng Mater Adv Technol 2015; 5:42–51.
30. Owen MJ. Why silicones behave funny. Chim Nouv 2005; 11:1–11.

Address correspondence to:
Newell R. Washburn
Department of Chemistry
Carnegie Mellon University
#814, Mellon College of Science
4400 Fifth Avenue
Pittsburgh, PA 15213

E-mail: washburn@andrew.cmu.edu

This article has been cited by:

1. Zhouquan Fu, Saman Naghieh, Cancan Xu, Chengjin Wang, Wei Sun, Xiongbiao Chen. 2021. Printability in extrusion bioprinting. *Biofabrication* **13**:3, 033001. [Crossref]
2. Paul S. Clegg. 2021. Characterising soft matter using machine learning. *Soft Matter* **17**:15, 3991-4005. [Crossref]
3. Daniel J. Shiwarski, Andrew R. Hudson, Joshua W. Tashman, Adam W. Feinberg. 2021. Emergence of FRESH 3D printing as a platform for advanced tissue biofabrication. *APL Bioengineering* **5**:1, 010904. [Crossref]
4. G. D. Goh, S. L. Sing, W. Y. Yeong. 2021. A review on machine learning in 3D printing: applications, potential, and challenges. *Artificial Intelligence Review* **54**:1, 63-94. [Crossref]
5. Daniela F. Duarte Campos, Laura De Laporte. 2021. Digitally Fabricated and Naturally Augmented In Vitro Tissues. *Advanced Healthcare Materials* **10**:2, 2001253. [Crossref]
6. Jennifer M. Bone, Christopher M. Childs, Aditya Menon, Barnabás Póczos, Adam W. Feinberg, Philip R. LeDuc, Newell R. Washburn. 2020. Hierarchical Machine Learning for High-Fidelity 3D Printed Biopolymers. *ACS Biomaterials Science & Engineering* **6**:12, 7021-7031. [Crossref]
7. Anja Conev, Eleni E. Litsa, Marissa R. Perez, Mani Diba, Antonios G. Mikos, Lydia E. Kavraki. 2020. Machine Learning-Guided Three-Dimensional Printing of Tissue Engineering Scaffolds. *Tissue Engineering Part A* **26**:23-24, 1359-1368. [Abstract] [Full Text] [PDF] [PDF Plus] [Supplementary Material]
8. R. Durga Prasad Reddy, Varun Sharma. 2020. Additive manufacturing in drug delivery applications: A review. *International Journal of Pharmaceutics* **589**, 119820. [Crossref]
9. Andrea Schwab, Riccardo Levato, Matteo D'Este, Susanna Piluso, David Eglin, Jos Malda. 2020. Printability and Shape Fidelity of Bioinks in 3D Bioprinting. *Chemical Reviews* **120**:19, 11028-11055. [Crossref]
10. Miss Anja Conev, Miss Eleni Litsa, Miss Marissa Perez, Dr. Mani Diba, Dr. Antonios G. Mikos, Prof. Lydia Kavraki. Machine Learning Guided 3D Printing of Tissue Engineering Scaffolds. *Tissue Engineering Part A* **0**:ja. . [Abstract] [PDF] [PDF Plus]
11. Eric Luis, Houwen Matthew Pan, Anil Kumar Bastola, Ram Bajpai, Swee Leong Sing, Juha Song, Wai Yee Yeong. 2020. 3D Printed Silicone Meniscus Implants: Influence of the 3D Printing Process on Properties of Silicone Implants. *Polymers* **12**:9, 2136. [Crossref]
12. Jingchao Jiang, Yongsheng Ma. 2020. Path Planning Strategies to Optimize Accuracy, Quality, Build Time and Material Use in Additive Manufacturing: A Review. *Micromachines* **11**:7, 633. [Crossref]
13. Riccardo Levato, Tomasz Jungst, Ruben G. Scheuring, Torsten Blunk, Juergen Groll, Jos Malda. 2020. From Shape to Function: The Next Step in Bioprinting. *Advanced Materials* **32**:12, 1906423. [Crossref]
14. Ali Zolfagharian, Akif Kaynak, Abbas Kouzani. 2020. Closed-loop 4D-printed soft robots. *Materials & Design* **188**, 108411. [Crossref]
15. Yang Wu, Dino J. Ravnic, Ibrahim T. Ozbolat. 2020. Intraoperative Bioprinting: Repairing Tissues and Organs in a Surgical Setting. *Trends in Biotechnology* . [Crossref]
16. Joohyun Kim, Jane A. McKee, Jake J. Fontenot, Jangwook P. Jung. 2020. Engineering Tissue Fabrication With Machine Intelligence: Generating a Blueprint for Regeneration. *Frontiers in Bioengineering and Biotechnology* **7**. . [Crossref]
17. Zeqing Jin, Zhizhou Zhang, Grace X. Gu. 2020. Automated Real-Time Detection and Prediction of Interlayer Imperfections in Additive Manufacturing Processes Using Artificial Intelligence. *Advanced Intelligent Systems* **2**:1, 1900130. [Crossref]
18. Glen Williams, Nicholas A. Meisel, Timothy W. Simpson, Christopher McComb. 2019. Design Repository Effectiveness for 3D Convolutional Neural Networks: Application to Additive Manufacturing. *Journal of Mechanical Design* **141**:11. . [Crossref]